

Nucleon Excited States in $N_f=2$ lattice QCD

C. Alexandrou,^{1,2} T. Korzec,³ G. Koutsou,² and T. Leontiou⁴

¹*Department of Physics, University of Cyprus, P.O. Box 20537, 1678 Nicosia, Cyprus*

²*The Cyprus Institute, P.O. Box 27456, 1645 Nicosia, Cyprus*

³*Institut für Physik, Humboldt Universität zu Berlin, Newtonstrasse 15, 12489 Berlin, Germany*

⁴*General Department, Frederick University, 1036 Nicosia, Cyprus*

We investigate the excited states of the nucleon using $N_f = 2$ twisted mass gauge configurations for pion masses in the range of about 270 MeV to 450 MeV and one ensemble of $N_f = 2$ Clover fermions at almost physical pion mass. We use two different sets of variational bases and study the resulting generalized eigenvalue problem. We present results for the two lowest positive and negative parity states.

I. INTRODUCTION

Understanding the excitation spectrum of hadrons and in particular that of the proton is still a challenge. In particular, the $P_{11}(1440\text{MeV})$ positive parity resonance known as the Roper, still remains a puzzle having a mass lower than the negative parity state $S_{11}(1535\text{MeV})$. This ordering is contrary to the prediction of constituent quark models where the negative parity is lower in mass than P_{11} . Lattice QCD simulations have recently reproduced the mass of the low-lying baryon states using gauge configurations with pions having mass close to the physical value [1, 2]. In these studies volume and cut-off effects have been taken into account by performing the calculation at different volumes and lattice spacings. Contrary to the low-lying baryon states the study of excited states has not yet reached the same level of maturity. In order to extract excited state energies, a robust analysis of simulation data keeping systematic errors under control is needed.

The study of excited states is mostly based on the variational principle, which was first applied to extract glueball masses [3]. One considers a number of interpolating fields as a variational basis and a generalized eigenvalue problem (GEVP) is defined, which yields the low-lying energy levels. The GEVP has been applied recently to study hadron spectroscopy by a number of lattice groups [4–8]. A crucial question of such an approach is the convergence of the energy levels to the true value. This was first addressed in a paper by Lüscher and Wolff [9] and recently by the Alpha-collaboration [10]. In this work, we explore the variational approach as put forward by the Alpha-collaboration to study the excited states of the nucleon in the positive and negative parity channels. We examine two types of nucleon interpolating fields as well as different levels of gaussian smearings. The approach proposed by the Alpha-collaboration is compared with the standard GEVP where the reference time t_0 is kept fixed at a small value. The main outcome of this comparison is that, within the current statistical accuracy typically used for baryon calculations, namely $\mathcal{O}(10^2)$ configurations, we do not see any improvements to the standard analysis. Having established at one ensemble of twisted mass fermions that

the standard approach performs equally well, we adopt it for the other ensembles. We analyze a total of five ensembles of $N_f = 2$ twisted mass fermions with pion mass in the range of about 270 MeV to 450 MeV and lattice spacing $a = 0.089$ fm determined from the nucleon mass [2]. Cut-off effects on the mass of the nucleon and hyperons were examined in Refs. [2, 11] respectively using two smaller lattice spacings. The conclusion was that cut-off effects were within the statistical errors and one could take the continuum limit assuming negligible $\mathcal{O}(a^2)$ contributions. Therefore, in this work, we limit ourselves to studying only one lattice spacing for twisted mass fermions. In addition, we analyze an ensemble of $N_f = 2$ Clover fermions with pion mass $m_\pi \sim 160$ MeV and lattice spacing $a \simeq 0.073$ fm.

The paper is organized as follows: In section II we give the details of the simulations; in section III we compare results using different variational basis and analysis approaches for an ensemble of twisted mass fermions with $m_\pi \sim 300$ MeV; in section IV we give our results, and in section V we summarize our findings and give our conclusions.

II. SIMULATION DETAILS

The input parameters of the calculation using $N_f = 2$ twisted mass fermions, namely β , L/a and $a\mu$ are summarized in Table I. These are the same configurations already used in the analysis of the low-lying baryon spectrum [11], where more details regarding the twisted mass formulation can be found. The corresponding lattice spacing a and the pion mass values, spanning a mass range from 270 MeV to 450 MeV, are taken from Ref. [2]. For the lattice spacing we take the value determined from the nucleon mass, which, taking into account the systematic error due to the chiral extrapolation, is consistent with the one extracted from f_π [12].

Apart from the twisted mass fermion ensembles given in Table I we also analyzed an ensemble of $N_f = 2$ Clover fermion configurations produced by the QCDSF collaboration. We use the $48^3 \times 64$ ensemble with near-physical pion mass of $m_\pi \simeq 160$ MeV, at $\beta = 5.29$ for which the lattice spacing has been determined to

$\beta = 3.9$, $a = 0.089(1)(5)$ fm from the nucleon mass				
$r_0/a = 5.22(2)$				
$24^3 \times 48$, $L = 2.05$ fm	$a\mu$	0.0040	0.0064	0.0085
	No. of confs	782	545	348
	m_π (GeV)	0.3131(16)	0.3903(9)	0.4470(12)
	$m_\pi L$	3.25	4.05	4.63
$32^3 \times 64$, $L = 2.74$ fm	$a\mu$	0.003	0.004	
	No. of confs	659	232	
	m_π (GeV)	0.2696(9)	0.3082(6)	
	$m_\pi L$	3.74	4.28	

TABLE I. Input parameters (β, L, μ) of our lattice calculation and corresponding lattice spacing (a) and pion mass (m_π). The value of the lattice spacing determined from f_π is $a = 0.0855(6)$ fm.

be $a = 0.0728(5)(19)$ fm [13]. This yields a value for $m_\pi L \simeq 2.8$. We smear the links that enter the Dirac operator with three iterations of APE smearing and set the clover term to its tree-level value i.e. $c_{SW} = 1$. Smearing the links in this way changes κ_{crit} . We therefore tune the value of the hopping parameter κ as described in [14] to match the pion mass in the unitary theory. A comparison of the pion and nucleon effective masses, $am_{\text{eff}}(t) \equiv \log[C(t)/C(t+1)]$, in the unitary theory and after tuning is shown in Fig. 1. As can be seen, the mass of the nucleon in the tuned theory agrees with the one obtained in the unitary theory. Note that one has to allow 10 time slices or about 0.7 fm to ensure that excited states have been sufficiently suppressed. Performing a double exponential fit yields a suppression factor of $\mathcal{O}(e^{-4})$ from the gap from the mass gap between the ground and excited state, which means there is a substantial overlap of the standard nucleon interpolating field with higher excited states.

III. THE VARIATIONAL METHOD

The standard extraction of the ground state energy from the large time limit of Euclidean two-point correlation functions relies on the fact that they are expressed as a sum of the energy eigenstates of QCD that exponentially decay as a function of the time with a rate proportional to the energy. The variational method provides an approach for extracting, besides the lowest energy state, the low-lying excited states from Euclidean correlation functions. A variational basis is constructed by using different interpolating fields χ with the quantum numbers of the particular state of interest, which in this work is the nucleon. Applying the variational principle one can determine the superposition of states that correspond to the low-lying nucleon states. One variational basis is obtained by considering two different spin combinations of

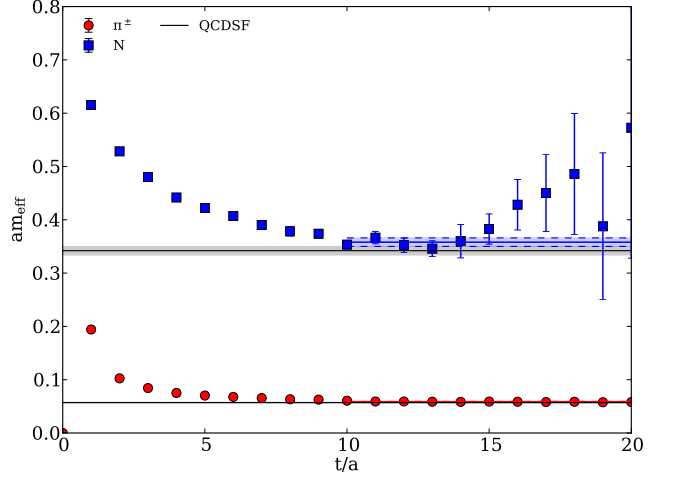


FIG. 1. The pion (red circles) and nucleon (blue squares) effective masses in the non-unitary setup as described in the text, compared to their values in the unitary theory (solid black line) computed by QCDSF [13]. The value of κ in the non-unitary setup was tuned to reproduce the pion mass in the unitary theory.

nucleon interpolating fields, namely

$$\chi_1 = (u^T C \gamma_5 d)u \text{ and } \chi_2 = (u^T C d)\gamma_5 u. \quad (1)$$

The local scalar-diquark nucleon interpolator, χ_1 , is well known to have a good overlap with the ground state of the nucleon, while the χ_2 interpolator, which vanishes in the non-relativistic limit, is believed to couple strongly to the first excitation of the nucleon, the Roper. In addition, the variational basis is enlarged by considering different gaussian smearings using similar parameters to those used in Ref. [10]. The correlation matrix considered here thus has the general form:

$$\begin{aligned} C_{a_i b_j}^\pm(t) &= \sum_{\mathbf{x}} \text{Tr} \left[\frac{1}{4} (1 \pm \gamma_0) \langle \chi_a^{(i)}(\mathbf{x}, t) \bar{\chi}_b^{(j)}(\mathbf{0}, 0) \rangle \right] \\ &= \sum_{n=0}^{\infty} e^{-E_n t} \text{Tr} \left[\frac{1}{4} (1 \pm \gamma_0) \langle 0 | \chi_a^{(i)} | n \rangle \langle n | \chi_b^{(j)} | 0 \rangle \right], \\ i, j &= 1, \dots, N \\ a, b &= 1, 2, \end{aligned} \quad (2)$$

where the trace is taken over Dirac indices and $C^+(t)$ ($C^-(t)$) yields the positive (negative) parity correlator. The states $|n\rangle$ are eigenstates of the Hamiltonian with $E_n < E_{n+1}$ and we have assumed that the temporal extent of the lattice is large enough to neglect boundary contributions. We note, however, that in our analysis we average over the forward and backward propagating nucleons. The indices i and j on the correlation matrix $C^\pm(t)$ correspond to different levels of gaussian smearing and a and b to χ_1 and χ_2 .

A. Variational basis with different gaussian smearing levels of χ_1

In this subsection we perform an analysis using a variational basis of χ_1 with a number of different smearing levels. The variational basis is constructed using N different gaussian smearing levels of this interpolating field. The GEVP is defined by the generalized eigen-equation

$$C(t)v_n(t, t_0) = \lambda_n(t, t_0)C(t_0)v_n(t, t_0), \quad n = 1, \dots, N, t > t_0, \quad (3)$$

where $E_n = \lim_{t \rightarrow \infty} -\partial_t \log \lambda_n(t, t_0)$. The corrections to E_n decrease exponentially like $e^{-\Delta E_n t}$ where $\Delta E_n = \min_{m \neq n} |E_m - E_n|$ [9] for fixed t_0 . In Ref. [9, 10] it was shown that if one varies t_0 such that $t_0 \geq t/2$ then the correction is $\mathcal{O}(e^{-\Delta E_{N,n} t})$ with $\Delta E_{m,n} = E_m - E_n$ ensuring a greater rate of convergence. In this section we examine the benefit of this relation for extracting the low-lying states in the nucleon sector. We apply gaussian smearing to each quark field, $q(\mathbf{x}, t)$ [15, 16], entering χ_1 . The smeared quark field is given by $q^{\text{smeared}}(\mathbf{x}, t) = \sum_{\mathbf{y}} F(\mathbf{x}, \mathbf{y}; U(t))q(\mathbf{y}, t)$ using the gauge invariant smearing function

$$F(\mathbf{x}, \mathbf{y}; U(t)) = (1 + \alpha H)^{n_s}(\mathbf{x}, \mathbf{y}; U(t)), \quad (4)$$

constructed from the hopping matrix understood as a matrix in coordinate, color and spin space

$$H(\mathbf{x}, \mathbf{y}; U(t)) = \sum_{i=1}^3 \left(U_i(\mathbf{x}, t) \delta_{\mathbf{x}, \mathbf{y} - a\hat{i}} + U_i^\dagger(\mathbf{x} - a\hat{i}, t) \delta_{\mathbf{x}, \mathbf{y} + a\hat{i}} \right). \quad (5)$$

Smearing is applied at the fermion source and sink. Following Ref. [10] we consider values of the smearing parameters $\alpha = 0.1$ and $n_s = 0, 22, 45, 67$ and 135. These smearing parameters produce a source with a root mean square (r.m.s.) radius in lattice units of 0, 1.96, 2.72, 3.25 and 4.48 respectively. These different smearing levels are labeled by the superscript $i = 1, \dots, 5$ on $\chi^{(i)}$. The resulting correlation matrices are symmetrized. We use 150 twisted mass fermion configurations with $\beta=3.9$, $a\mu = 0.004$ or $m_\pi \sim 308$ MeV on a $32^3 \times 64$ lattice.

Let us first examine the advantage of using these different smearing levels. We consider several different correlation matrices of the positive parity correlator $C_{1_i 1_j}^+(t)$ constructed from $\chi_1^{(i)}$ for different smearing levels i in order to examine both the role of varying n_s and/or the dimensionality of the GEVP. In Fig. 2 we show the effective mass for the ground and first excited states resulting from a GEVP analysis of all possible 3×3 correlation matrices fixing $t_0/a = 1$. We are looking for the combination of interpolating fields that give the fastest convergence to the two-lowest levels E_0 and E_1 i.e. to the earliest onset of a plateau behavior. From this analysis it is evident that using the higher smearing levels slightly improves convergence. Nevertheless, the overall quality of the plateaus after time-slice $t/a = 6$ is similar allowing

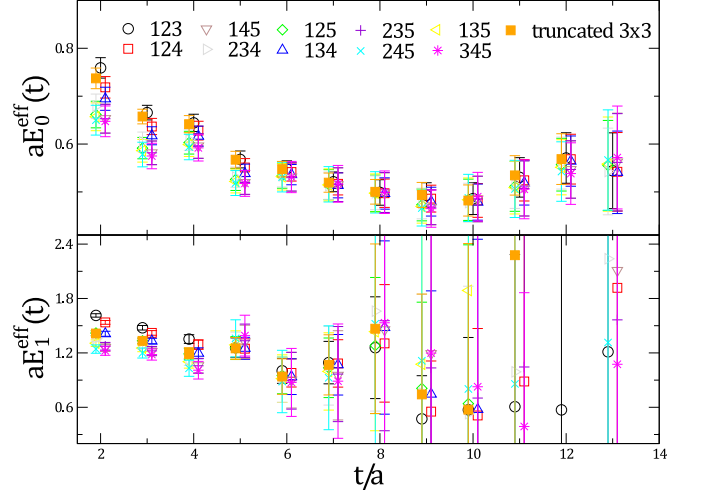


FIG. 2. The effective mass for the ground (E_0) and first excited (E_1) states resulting from a 3×3 GEVP. A 3×3 correlation matrix was constructed out of different interpolating fields $\chi_1^{(i)}$ by applying a different number of gaussian smearing iterations on χ_1 . The numbers in the legend give the combination of the three values of n_s used to construct the basis. The effective energy levels resulting from a truncated 3×3 GEVP constructed using Eq. (6) are also shown. This analysis was carried out using 150 configurations of twisted mass fermions at $\beta=3.9$, $a\mu = 0.004$ ($m_\pi \sim 308$ MeV) on a $32^3 \times 64$ lattice.

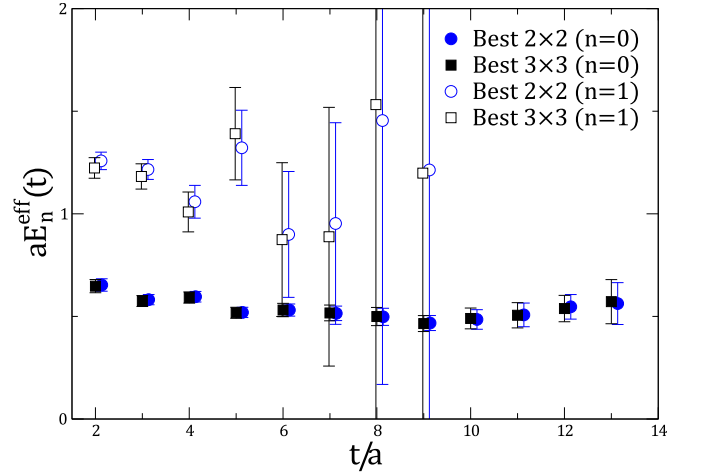


FIG. 3. The effective mass for the ground ($n = 0$) and first ($n = 1$) excited states from the best choice of 2×2 and 3×3 GEVPs corresponding to the highest level of Gaussian smearing i.e. from $\{\chi_1^{(4)}, \chi_1^{(5)}\}$ for the 2×2 GEVP and $\{\chi_1^{(3)}, \chi_1^{(4)}, \chi_1^{(5)}\}$ for the 3×3 GEVP. The test was carried out using 150 configurations of the twisted mass ensemble with $\beta=3.9$, $a\mu = 0.004$ ($m_\pi \sim 308$ MeV) on a $32^3 \times 64$ lattice

extraction of the mass with all ten possible 3×3 combinations. Apart from making a choice of the best basis by trying different combinations of gaussian smearing we also try a truncation scheme where the 5×5 correlation matrix is projected to an $m \times m$ matrix, $C^{m \times m}(t)$, using

the m eigenvectors belonging to the m largest eigenvalues of $C(t_0)$ with $m < 5$ as follows:

$$C^{N \times N}(t_0)b = \Lambda b, \quad C_{kj}^{m \times m}(t) = b_{ki}^\dagger C^{N \times N}(t)b_{ij}, \\ k, j = 1, \dots, m, \quad i = 1, \dots, N, \quad (6)$$

where $\Lambda_{jk} = \delta_{jk}e^{-E_j t_0}$ is an $N \times N$ matrix with the eigenvalues of $C^{N \times N}(t_0)$ as its diagonal elements and b an $N \times N$ matrix with the corresponding eigenvectors. We additionally tried this truncation scheme with various values of t_0/a , namely $t_0/a = 1, \dots, 4$ and results obtained are statistically equivalent. The resulting effective masses extracted from the truncated 3×3 matrix, are plotted in Fig. 2. As can be seen, they do not show any improved convergence, in particular in comparison with those extracted from the optimal 3×3 correlation matrix, i.e. the “345” combination, constructed with $\chi_1^{(3)}, \chi_1^{(4)}$ and $\chi_1^{(5)}$.

The effect of reducing the dimension of the GEVP to 2×2 can be seen in Fig. 3. The quality of the plateaus for the first two states is not affected as compared to those extracted using the optimal 3×3 correlation matrix.

In Fig. 4 we compare the GEVP results to the standard method of extracting the effective mass using a single interpolating field $\chi_1^{(i)}$, or equivalently to the trivial 1×1 GEVP in the case of the ground state. As can be seen, using just the $\chi_1^{(5)}$ interpolating field yields the same quality plateau as that obtained from the 3×3 correlation matrix analysis. This is to be expected since this smearing is optimal for the nucleon ground state.

For the two lowest states in the positive channel we also study the resulting eigenvectors in order to understand/verify the mixture of the various $\chi_1^{(i)}$ contributing in the best interpolating field for each state. Identifying the optimum combination of $\chi_1^{(i)}$ extracted from the GEVP analysis is useful if one wants to calculate the matrix elements of any operator using the optimal interpolating field that best suppresses the contribution of excited states.

In Fig. 5 the three components V_1, V_2 and V_3 of the eigenvector for the ground and excited states in the positive parity channel determined from the optimal 3×3 correlation matrix constructed from χ_1 with smearing iterations $n_s = 45, 67$ and 135 are displayed. The interpolating field with the maximum overlap with the ground state is given by $\chi_{\text{eff}} = \tilde{v}_1 \chi_1^{(5)} + \tilde{v}_2 \chi_1^{(4)} + \tilde{v}_3 \chi_1^{(3)}$, where \tilde{v} is the large-time limit of $\tilde{v}(t_0) = \lim_{t \rightarrow \infty} V(t, t_0)$. It is evident that most of the contribution comes from the components \tilde{v}_1 and \tilde{v}_2 , while \tilde{v}_3 has very little contribution (an order of magnitude less). This is in agreement with the previous observation that a 2×2 GEVP with $n_s = 67$ and 135 is adequate for these first two states. The ground state is dominated by the highest smearing level (\tilde{v}_1) and for the first excited state the contribution from \tilde{v}_2 increases.

Let us next vary t_0 as suggested in Ref. [10], where it was shown that this lead to an improvement in the determination of the ground state by successfully suppressing

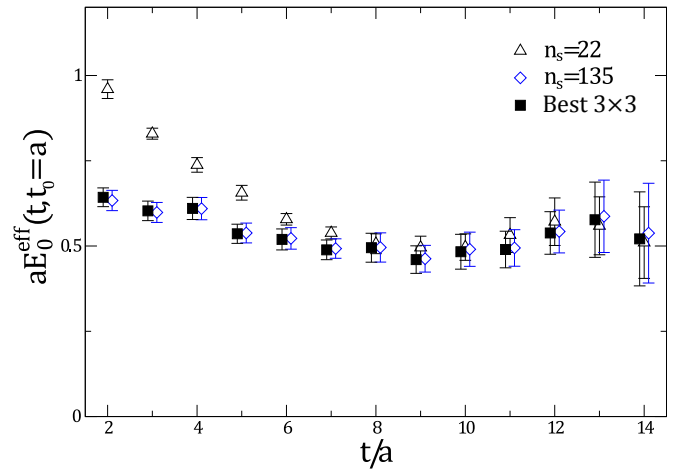


FIG. 4. The effective mass for the ground state for $t_0/a = 1$. Results are shown for the GEVP with the best choice of 3×3 using different gaussian smearings on $\chi_1^{(i)}$ with $i = 3, 4, 5$ and from the correlation function $C_{1_2 1_2}$ and $C_{1_5 1_5}$.

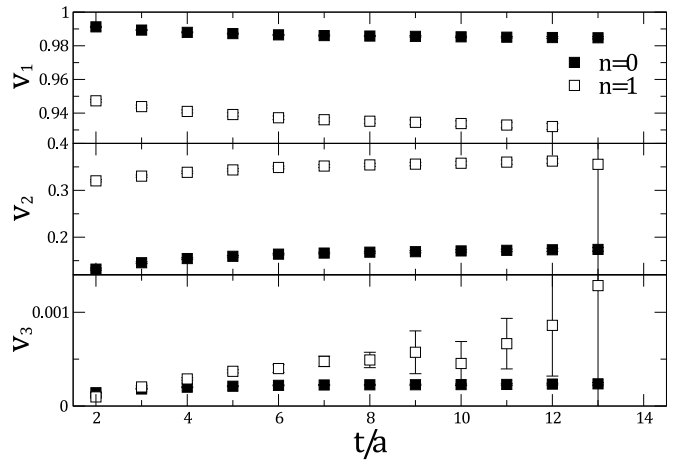


FIG. 5. The components of the eigenvector for the ground and first excited states at $t_0 = 1$. Results are shown for a GEVP with the optimal 3×3 correlator, $C_{1_i 1_j}$, $i, j = 3, 4, 5$.

excited state contamination for certain mesonic systems. In Fig. 6 we show results obtained at fixed $t_0/a = 1$ as well as results obtained by varying t_0 . Within the statistical accuracy of our analysis, we see consistent results for the three values of $t_0/a = 1, 3$, and 5 considered. Furthermore, we allow t_0 to vary for every value of t and, in particular, we apply the condition $t_0 \geq t/2$ as suggested in Ref. [10]. We show results for the ground and first excited states in the positive parity channel for the case $t_0 = t/2$, where we observe no change in the plateau range within the present statistics. For these nucleon states and within the present accuracy, this analysis does not show an improvement. Our conclusion is that for the low-lying nucleon spectrum, where the energy gap is not particularly small, the variation of t_0 that has been shown in Ref. [10] to reduce the systematic error is not observed

here at least within the limitation of our statistics. Thus, for our case, one can efficiently extract the energy spectrum from the effective mass plateaus at a fixed value of t_0 . In what follows we will fix $t_0/a = 1$.

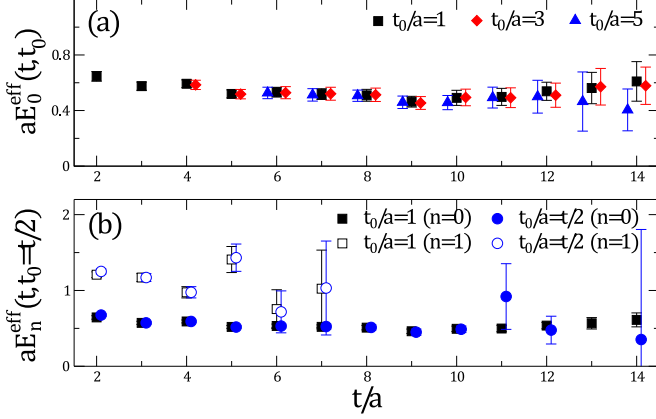


FIG. 6. (a) The effective mass for the ground state for various choices of t_0 . Results are shown for the best choice of 3×3 GEVP. (b) The effective mass for the ground and first excited states with a fixed value for t_0 (squares) and with the condition $t_0 = t/2$ (circles) for the ground (filled symbols) and first excited state (open symbols). Values have been slightly shifted in time in order to aid the comparison.

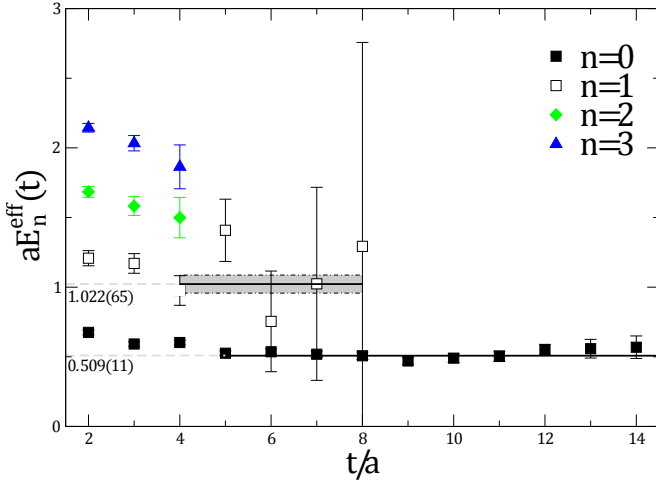


FIG. 7. The spectrum when using $\chi_1^{(i)}$ for a 5×5 GEVP using 150 configurations at $\beta=3.9$, $a\mu = 0.004$ ($m_\pi \sim 308\text{MeV}$) on a $32^3 \times 64$ lattice. The basis set of interpolating fields consisted of $n_s = 0, 22, 45, 67$ and 135 Gaussian smearing iterations. The solid lines and bands show the fitted effective mass and jackknife error.

From the above analysis it is clear that the merit of the variational approach lies in the extraction of excited states, whereas the ground state is equally well obtained using the optimally smeared interpolating function $\chi_1^{(5)}$. In Fig. 7 we analyze the 5×5 GEVP to extract the nucleon spectrum. Despite the low statistics used for this test case, we are able to obtain effective mass plateaus

$m_{\text{eff}}(n)$ for the ground-state ($n=0$) and the first excited state ($n=1$) and an indication for the second and third excited states ($n=2$ and $n=3$).

B. Combining both χ_1 and χ_2

In the preceding subsection we used a variational basis constructed from different smearing levels of the χ_1 interpolating field. In this section, we extend the investigation by combining both $\chi_1^{(i)}$ and $\chi_2^{(i)}$ each with two different smearing levels: a local source and $n_s=135$ with $\alpha=0.1$, i.e. using the interpolating fields: $\chi_1^{(1)}, \chi_2^{(1)}, \chi_1^{(5)}$ and $\chi_2^{(5)}$. We thus have a 4×4 correlation matrix. We examine the same ensemble as in the previous section. In Fig. 8 we display a comparison of this 4×4 basis with the full 5×5 basis of the previous section. This is done for the ground and first excited states in the positive parity channel. The effective mass plateaus are statistically equivalent for both basis sets. In addition we compare to the 2×2 problem constructed using the basis $\{\chi_1^{(5)}, \chi_2^{(5)}\}$. As can be seen this yields results consistent with the 4×4 and 5×5 systems. Furthermore, by examining Fig. 9, where we illustrate the effective mass of the two lowest states extracted from this 4×4 GEVP to those obtained from the correlators $C_{15\ 15}$ and $C_{25\ 25}$ i.e. using alone $\chi_1^{(5)}$ or $\chi_2^{(5)}$ at both source and sink, we find that the effective masses coincide. For the ground state this was already demonstrated in Fig. 4. The new result is that $\chi_2^{(5)}$ yields the first *excited state* in the positive parity channel.

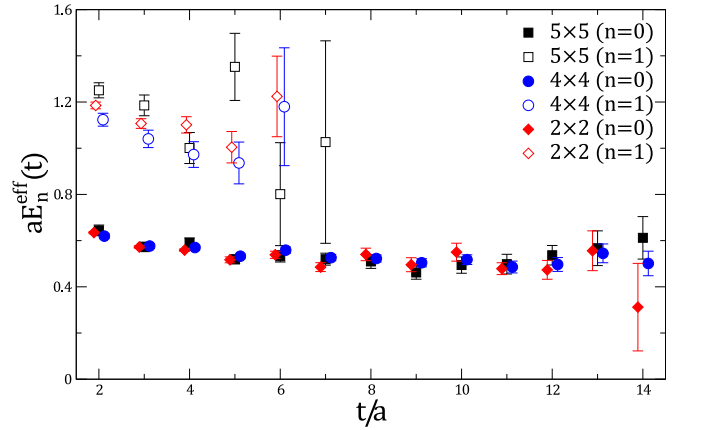


FIG. 8. The effective mass for the ground and first excited states for the positive parity channel for $\beta=3.9$, $a\mu = 0.004$ on a $32^3 \times 64$ lattice. The 5×5 system is obtained from $C_{1_i 1_j}$ with $i, j \leq 5$; 4×4 corresponds to the that obtained using $C_{a_i b_j}$ with $a, b = 1, 2$ and $i, j = 1, 5$ and 2×2 to the system obtained from $C_{a_5 b_5}$ with $a, b = 1, 2$. 150 configuration are used for the 5×5 GEVP and 280 for the 4×4 and the 2×2 version.

This important conclusion is corroborated by considering the results shown in Fig. 10 where we compare the ef-

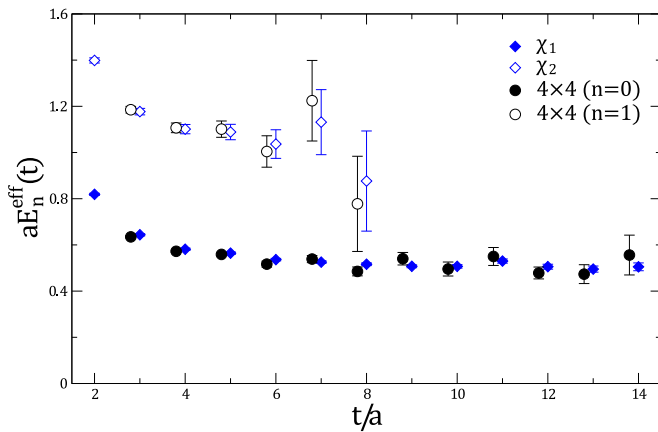


FIG. 9. The effective mass for the ground and first excited states in the positive channel. The effective masses from the interpolators $\chi_1^{(5)}$ and $\chi_2^{(5)}$ is compared with the results obtained from the same 4×4 GEVP as explained in Fig. 8.

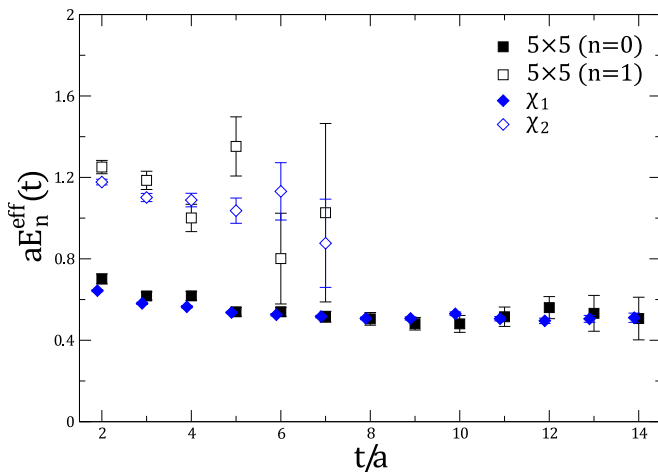


FIG. 10. The effective mass for the ground and first excited states in the positive channel. The effective masses from the interpolators $\chi_1^{(5)}$ and $\chi_2^{(5)}$ is compared with the results obtained from the 5×5 GEVP as explained in Fig. 8.

fective mass extracted from a GEVP analysis of $C_{1_i 1_j}(t)$, $i, j \leq 5$ with the effective mass when using just $\chi_a^{(5)}$ i.e. $C_{a_5 a_5}$ with $a = 1, 2$. It is evident that the first excited state obtained from the GEVP is identical to the ground state extracted from $C_{2_5 2_5}$, carrying smaller statistical errors, a result that we will use in order to further examine the first excited state. This illustrates that χ_2 strongly couples to the first excited nucleon state but not to the ground state.

For the case of the negative parity states, it is important to note that the negative parity interpolating operator in Eq. 2 has a non-zero overlap with the two particle S-wave state which consists of a nucleon and a pion. At the physical point, this state has lower energy than the negative parity nucleon. To know *a priori* if and at which

pion mass the negative parity nucleon and the πN state cross requires knowledge of the pion mass dependence of the negative parity nucleon. In Fig. 11, we show the ground and first excited states obtained from a 4×4 and 2×2 GEVP. As in the case of Fig. 8, the 4×4 GEVP is solved using the basis $\{\chi_1^{(1)}, \chi_1^{(5)}, \chi_2^{(1)}, \chi_2^{(5)}\}$, while the 2×2 using $\{\chi_1^{(5)}, \chi_2^{(5)}\}$. As can be seen the ground and first excited states are statistically equivalent when obtained by solving the GEVP of either size.

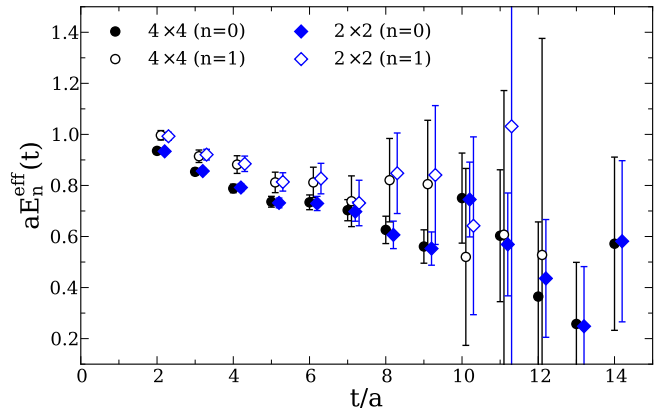


FIG. 11. The nucleon ground (filled symbols) and first excited state (open symbols) in the negative parity channel, evaluated via a 4×4 GEVP (black circles) and a 2×2 GEVP (blue diamonds). The interpolator bases used for these two GEVPs are the same as those used in Fig. 8 for the same GEVP size. 240 configurations were used for this test.

Having verified that the 2×2 GEVP yields the same energies for the ground and first excited states of the negative parity as the 4×4 GEVP does, we will hereof use the 2×2 GEVP to resolve the ground and first excited negative parity states for all other pion masses. Knowing which of these is the multi-particle state would require investigating the dependence of the two energy levels on the lattice volume, which is beyond the scope of this work. We therefore compare the two energy states with the sum of the nucleon and pion mass, and from this infer which is the negative parity nucleon state. Further examples of the effective masses obtained for the negative parity states using the 2×2 GEVP are given in Figs. 12 and 13, discussed in the following section.

IV. THE LOW-LYING NUCLEON SPECTRUM

In the previous section we have shown that if we are interested in the first excited positive parity states of the nucleon both the variational analysis and the interpolating fields $\chi_1^{(5)}$ and $\chi_2^{(5)}$ yield equivalent results for the ground and first excited state. Since in the rest of this work we will be interested in the first excited state we minimize the computational effort and carry out an investigation of the ground-state and the first excited state of the nucleon using the correlators constructed with χ_1 and

χ_2 with a single smearing level. We note that, to minimize computational resources, we reuse existing forward propagators, namely those used in [11]. These propagators were created with smearing parameters $n_s=50$ and $\alpha=4.0$, which yield an r.m.s. radius consistent with the parameters $n_s=135$, $\alpha=0.1$ which were used in the preceding section and labeled $\chi^{(5)}$. We nevertheless label this new smearing level differently, i.e. as $\chi^{(6)}$. Equivalently, for the negative parity states, we solve the 2×2 GEVP constructed from $C_{a_6 b_6}^-$ with $a, b = 1, 2$, as already discussed. We also note that results presented from here on have been obtained with the statistics listed in Table I.

In Figs. 12 and 13 we show the effective masses for both positive and negative parity states, for a twisted mass ensemble and for the Clover ensemble analyzed in this work. Note that the twisted mass ensemble used in Fig. 12 is the same as that used in Fig. 11 however with almost three times more statistics; in Fig. 11 the purpose was to perform a test for GEVPs with different bases and therefore less statistics were utilized to speed-up the calculation. As can be seen from Figs. 12 and 13, a plateau region can be identified for both the positive and negative parity states and the twisted mass fermion and clover ensembles respectively. The effective masses for the other twisted mass fermion ensembles display a similar behavior.

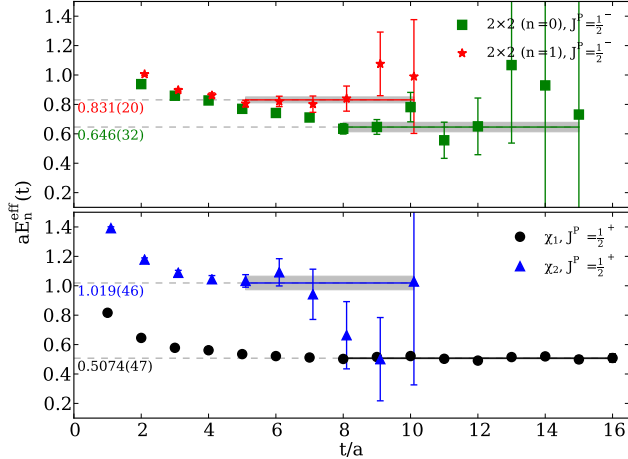


FIG. 12. The effective mass when using the $\chi_1^{(6)}$ and $\chi_2^{(6)}$ interpolating fields for the positive parity states (lower panel, $J^P = \frac{1}{2}^+$), and the 2×2 GEVP using $C_{a_6 b_6}^-$ with $a, b = 1, 2$, for the negative parity states (top panel, $J^P = \frac{1}{2}^-$). The results are for the ensemble with $\beta=3.9$, $a\mu = 0.004$ on a $32^3 \times 64$ lattice. The errors were obtained by the jackknife procedure.

The results for all of the ensembles of Table I and the single Clover ensemble are displayed in Fig. 14. For the nucleon mass we apply continuum chiral perturbation theory to extrapolate lattice results to the physical pion mass, omitting the Clover point from the fit. We use SU(2) heavy baryon chiral perturbation theory (HB χ PT)

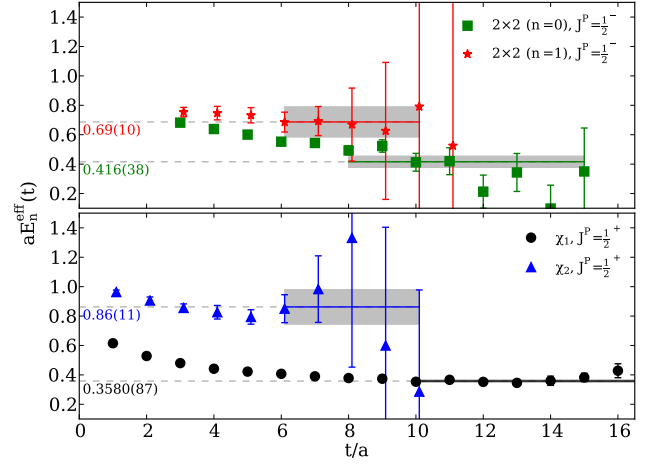


FIG. 13. The effective masses of the ground and first excited nucleon states for both positive and negative parity, for the $N_f = 2$ Clover lattice at $m_\pi \simeq 160$ MeV. The rest of the notation is the same as in Fig. 12

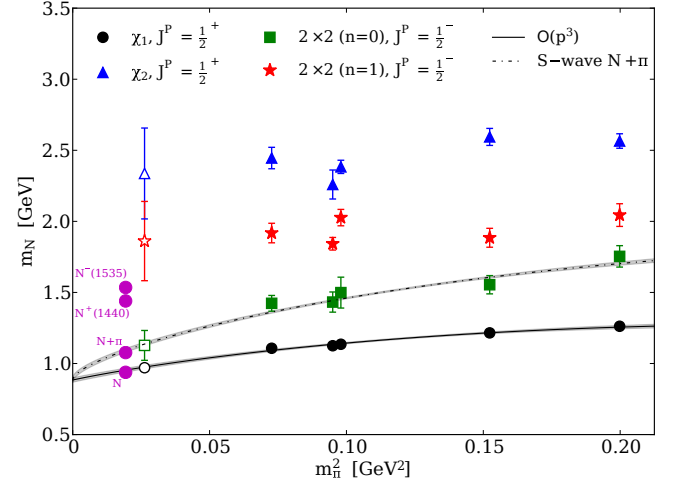


FIG. 14. The first positive and negative parity states measured in our different gauge ensembles. The twisted mass ensembles are plotted with filled symbols, while the results from the single Clover ensemble are denoted with the open symbols. We show chiral extrapolations for the nucleon ground state to the $\mathcal{O}(p^3)$ result of Eq. 7 using only the twisted mass fermions data. The dashed line is the resulting curve obtained by adding the pion mass to the $\mathcal{O}(p^3)$ curve. Physical masses for the different states are indicated by the magenta circles.

to $\mathcal{O}(p^3)$ given by

$$m_N(m_\pi) = m_N^{(0)} - 4c_N^{(1)} m_\pi^2 - \frac{3g_A^2}{16\pi f_\pi^2} m_\pi^3. \quad (7)$$

Since the lattice spacing was fixed using the nucleon mass it is no surprise that the curve passes through the physical value. However, the fact that it also passes through the result obtained with clover fermions is a non-trivial confirmation of the pion mass dependence of the nucleon

mass. In the figure we also show a curve obtained by adding the pion mass to the curve describing the nucleon mass. As can be seen, for all pion masses considered here, the negative parity ground state is consistent with the mass of the pion plus nucleon, indicating that this is the two particle πN state in an S-wave configuration.

In Figs. 15 and 16 we compare the results of this work with three other calculations available in the literature. Namely, we compare with the result using a Clover improved fermion action by the CSSM collaboration [19] with $a \simeq 0.09$ fm, a calculation using anisotropic Clover lattices by the Hadron Spectrum Collaboration [20] with spatial lattice spacing $a_s = 0.123$ fm and a calculation using the Chirally Improved Dirac Operator by the Bern-Graz-Regensburg (BGR) collaboration [21] and lattice spacings between 0.13 and 0.14 fm. We note that the lattice spacings for the two latter calculations are notably larger than those used in this work giving rise to issues about cut-off effects.

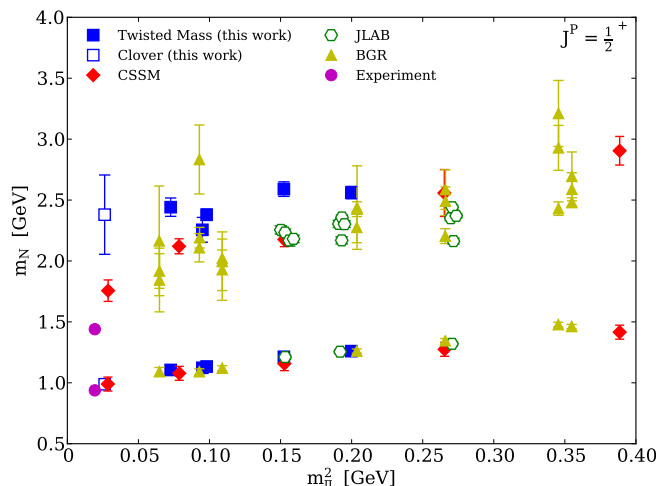


FIG. 15. The positive parity states of this work (filled and open squares) compared with results from other groups, that include a $N_f = 2 + 1$ Clover improved fermion calculation by the CSSM collaboration [19] (red diamonds), a calculation using anisotropic clover lattices by the Hadron Spectrum Collaboration [20] (open hexagons) and a calculation using the Chirally Improved Dirac Operator by the Berlin-Graz-Regensburg (BGR) collaboration [21] (yellow triangles).

The first observation is that all lattice results are in agreement in the case of the mass of the nucleon. Furthermore, in all cases results using twisted mass and Clover fermions are consistent. The second major observation is that our data for the first excited state of the nucleon in the positive parity channel are too high to be identified with the Roper. In fact all lattice data except the ones from the CSSM Collaboration are incompatible with the Roper. Our result using Clover fermions at $m_\pi \sim 160$ MeV remains high and shows no indication of converging to the mass of the Roper unlike the result from the CSSM collaboration. We do not observe a sharp change of slope as we decrease the pion mass as

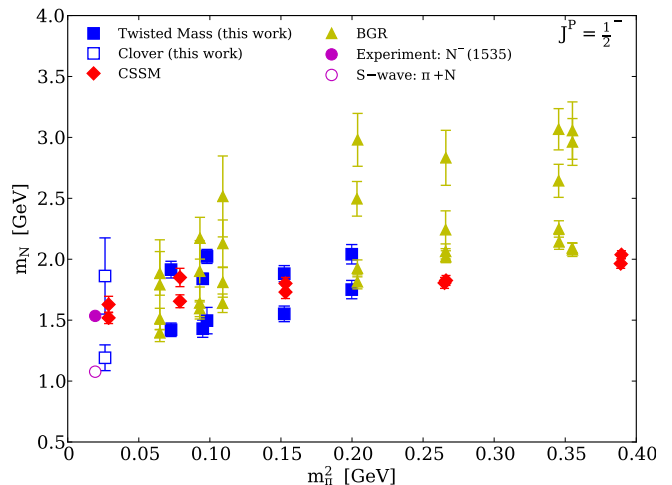


FIG. 16. The negative parity states of this work compared with calculations from other groups using the same notation as in Fig. 15.

observed in Ref. [19] and therefore it is unlikely that this discrepancy can be totally due to volume effects, since both our Clover calculation and the one in Ref. [19] are on lattices of comparable pion mass and physical lattice extent. In the negative parity channel our results are consistent with the ones from the BGR collaboration. We can clearly see that for all pion masses considered the negative parity ground state is consistent with a πN state in an S-wave. To the statistical accuracy available to us, the first excited negative parity state appears to be converging to $N^-(1535)$, however the errors are too large to draw concrete conclusions. It is clear from this analysis that extracting the excited states is much more challenging and more work is needed to fully understand the low-lying spectrum of the nucleon.

V. CONCLUSIONS

In this work we have applied the variational method to investigate the excited states of the nucleon. Two sets of variational bases were used and the analysis of the resulting GEVP was performed using the standard approach of fixing t_0 as well as by varying t_0 such that $t_0 \geq t/2$ as advocated in Ref. [10]. Within the current statistical accuracy, we found that for the nucleon excited states no observable improvement is obtained as compared to fixing t_0 . Limiting ourselves to the first excited state of the nucleon in the positive parity channel suffices to use the χ_1 and χ_2 interpolating fields with the optimal smearing. The former couples strongly to the ground state of the nucleon whereas the latter to the first excited positive parity state. Using these two interpolating fields we did an analysis using $N_f = 2$ dynamical fermion configurations reaching almost physical pion mass. Even at the lightest pion mass of 160 MeV we see no evidence for the

Roper. This is in agreement with most other lattice calculations shown in Fig 15 and may indicate that the interpolating fields used have small overlap with this state. In the negative parity state our result at $m_\pi = 160$ MeV is consistent with the mass of $N^-(1535)$.

Addendum: After the completion of this work the CSSM collaboration updated the results shown in this paper (Figs. 15 and 16) in Ref. [22].

ACKNOWLEDGMENTS

We would like to thank R. Sommer for a fruitful discussion. Numerical calculations have used the Cy-Tera facility of the Cyprus Institute under the project

Cy-Tera (NEA ΥΠΟΔΟΜΗ/ΣΤΡΑΤΗΓΙΚΗ/0308/31), first access call (project lspro113s1) and third access call (project lsprob115s1). In addition, this work was granted access to the HPC system “Lindgren” of KTH Stockholm, made available within the Distributed European Computing Initiative by the PRACE-2IP, receiving funding from the European Communitys Seventh Framework Programme (FP7/2007-2013) under grant agreement RI-283493. We thank the staff members of both sites for their kind and sustained support. This work is supported in part by the Cyprus Research Promotion Foundation under contracts KY-Γ/0310/02/, the Research Executive Agency of the European Union under Grant Agreement number PITN-GA-2009-238353 (ITN STRONGnet) and the FP7 infrastructures-2011-1 project HadronPhysics3 under Grant Agreement number 283286.

-
- [1] S. Durr et al., *Science* **322**, 1224 (2008).
 - [2] C. Alexandrou et al. (European Twisted Mass Collaboration), *Phys. Rev.* **D78**, 014509 (2008), 0803.3190.
 - [3] C. Michael and I. Teasdale, *Nucl.Phys.* **B215**, 433 (1983).
 - [4] S. Basak, R. Edwards, G. Fleming, K. Juge, A. Lichtl, et al., *Phys.Rev.* **D76**, 074504 (2007), 0709.0008.
 - [5] C. Gattringer, L. Y. Glozman, C. Lang, D. Mohler, and S. Prelovsek, *Phys.Rev.* **D78**, 034501 (2008), 0802.2020.
 - [6] C. Gattringer, C. Hagen, C. Lang, M. Limmer, D. Mohler, et al., *Phys.Rev.* **D79**, 054501 (2009), 0812.1681.
 - [7] M. Mahbub, A. O. Cais, W. Kamleh, D. B. Leinweber, and A. G. Williams, *Phys.Rev.* **D82**, 094504 (2010), 1004.5455.
 - [8] J. Bulava, R. Edwards, E. Engelson, B. Joo, H.-W. Lin, et al., *Phys.Rev.* **D82**, 014507 (2010), 1004.5072.
 - [9] M. Luscher and U. Wolff, *Nucl.Phys.* **B339**, 222 (1990).
 - [10] B. Blossier, M. Della Morte, G. von Hippel, T. Mendes, and R. Sommer, *JHEP* **0904**, 094 (2009), 0902.1265.
 - [11] C. Alexandrou et al. (ETM Collaboration), *Phys. Rev.* **D80**, 114503 (2009), 0910.2419.
 - [12] C. Urbach (European Twisted Mass Collaboration), *PoS LAT2007*, 022 (2007), 0710.1517.
 - [13] G. Bali, P. Bruns, S. Collins, M. Deka, B. Glasle, et al., *Nucl.Phys.* **B866**, 1 (2013), 1206.7034.
 - [14] S. Durr, G. Koutsou, and T. Lippert (2012), 1208.6270.
 - [15] S. Gusken, *Nucl. Phys. Proc. Suppl.* **17**, 361 (1990).
 - [16] C. Alexandrou, S. Gusken, F. Jegerlehner, K. Schilling, and R. Sommer, *Nucl. Phys.* **B414**, 815 (1994), hep-lat/9211042.
 - [17] M. Mahbub, A. O. Cais, W. Kamleh, B. G. Lasscock, D. B. Leinweber, et al., *Phys.Lett.* **B679**, 418 (2009), 0906.5433.
 - [18] M. S. Mahbub, W. Kamleh, D. B. Leinweber, P. J. Moran, and A. G. Williams (CSSM Lattice collaboration), *Phys.Lett.* **B707**, 389 (2012), 1011.5724.
 - [19] M. Mahbub, W. Kamleh, D. Leinweber, P. Moran, and A. Williams, *AIP Conf.Proc.* **1441**, 293 (2012).
 - [20] R. G. Edwards, J. J. Dudek, D. G. Richards, and S. J. Wallace, *Phys.Rev.* **D84**, 074508 (2011), 1104.5152.
 - [21] G. P. Engel, C. Lang, D. Mohler, and A. Schaefer (2013), 1301.4318.
 - [22] M. S. Mahbub, W. Kamleh, D. B. Leinweber, P. J. Moran, and A. G. Williams (2013), 1302.2987.